Suppression of Plasma Turbulence During Optimized Shear Configurations in JET

G. D. Conway, D. N. Borba, B. Alper, D. V. Bartlett, C. Gormezano, M. G. von Hellermann, A. C. Maas, V. V. Parail, P. Smeulders, and K-D. Zastrow

JET Joint Undertaking, Abingdon, Oxfordshire OX14 3EA, United Kingdom

(Received 24 May 1999)

Correlation of density turbulence suppression and reduced plasma transport is observed in the internal transport barrier (ITB) region of JET tokamak discharges with optimized magnetic shear. The suppression occurs in two stages. First, low frequency turbulence and ion transport are reduced across the plasma core by a toroidal velocity shear generated by intense auxiliary heating. Then with the ITB formation, high frequency turbulence and electron transport are reduced locally within the steep pressure gradient region of the ITB.

PACS numbers: 52.55.Fa, 52.35.Ra, 52.70.Gw

Much effort has been spent in recent years in developing alternative scenarios for operating tokamak fusion reactors. One particular scenario involves reversing or reducing the central magnetic shear to form an internal transport barrier (ITB). The result is reduced plasma core energy transport and enhanced fusion performance [1–7]. It is believed that ITBs may be formed through a combination of $\mathbf{E} \times \mathbf{B}$ velocity shear and magnetic shear stabilization of plasma turbulence and instabilities [8].

In this Letter we present results from Joint European Torus (JET) optimized shear discharges [5] showing that electrostatic turbulence suppression during ITB formation occurs in two stages. First low frequency turbulence is reduced across the plasma core, coinciding both spatially and temporarily with a region of strong toroidal velocity shear and reduced ion transport. Then high frequency turbulence is locally suppressed around the ITB region, coinciding with reduced electron transport.

The turbulence measurements were made using a system of X-mode reflectometers consisting of two, dual-channel toroidal correlation reflectometers at 75 GHz (covering plasma outboard edge) and 105 GHz (core and inboard edge), and a 92–96 GHz swept frequency radial correlation reflectometer (plasma core) [9]. Reflectometry is a powerful tool for measuring density fluctuations [10]. The highly localized reflection of the microwave beam gives excellent spatial localization. Measurements can be made throughout the plasma as the reflection layer location depends on the launched microwave frequency, the toroidal magnetic field B_T, plasma current I_p, and plasma density n_e. Reflectometers are primarily sensitive to long wavelength transverse fluctuations, i.e., poloidal wavelengths greater than the reflectometer beam radius w. For the JET reflectometers $w \sim 5$ cm and so are predominately sensitive to wave numbers $k_\perp < 1.2\ \mathrm{cm}^{-1}$. Also, unlike microwave scattering diagnostics, reflectometers are not susceptible to Doppler frequency shifts, unless there are substantial antenna misalignments [11].

Spatially, the turbulence in optimized shear discharges can be separated into three regions: outside the ITB (edge), around the ITB gradient, and inside the ITB (core). The turbulence behaves differently in each region. The core turbulence (ITB and within) evolves through four distinct phases: (1) Ohmic breakdown; (2) L-mode preheat, using ion cyclotron resonance heating (ICRH) to slow the current penetration and control the q profile evolution; (3) main heating using combined coinjected (parallel to I_p) neutral beam injection (NBI) and ICRH; and (4) the ITB formation. The edge turbulence by contrast shows little variation as the discharge evolves.

Figure 1 shows time traces of typical plasma parameters from a $B_T \approx 3.4$ T, $I_p \approx 3.4$ MA (peak) optimized shear discharge No. 46 727. This discharge was selected to illustrate the behavior of the turbulence for two reasons: (1) The formation of the ITB is delayed by almost 1 s due to the uneven coupling of the ICRH power (keeping the input heating power below the ITB threshold), allowing the effects of the ITB to be clearly separated from those due to the NBI. (2) During the ITB phase a reflectometer cutoff layer (92 GHz) remains located within the ITB gradient region at $R \sim 3.55$ m.

Figure 2 shows the spectral evolution of the core turbulence measured with this 92 GHz reflectometer channel. The spectrogram begins with the ICRH preheat phase, at 3.5 s into the discharge, and is dominated by large amplitude low frequency turbulence ($f < 50$ kHz). Compared to the preceding Ohmic phase the low ICRH power (2 MW) has little effect on the core or edge turbulence. However, its main effect is to generate large amplitude core localized toroidal Alfvén eigenmodes between 100 to 200 kHz together with lower frequency modes around 20 kHz.

The main part of the discharge in Fig. 2 begins at 4.7 s with the high power heating phase, consisting of combined NBI and ICRH with total power exceeding 15 MW. The power is usually stepped up in two stages to delay the formation of an H-mode during the I_p ramp. The spectrogram shows a sudden transformation in the core turbulence. The spectrum rapidly broadens with frequencies spreading up to $f > 300$ kHz followed by a complete suppression of low frequency turbulence. Note that the high frequency density turbulence increases throughout the plasma (edge

 © 2000 The American Physical Society

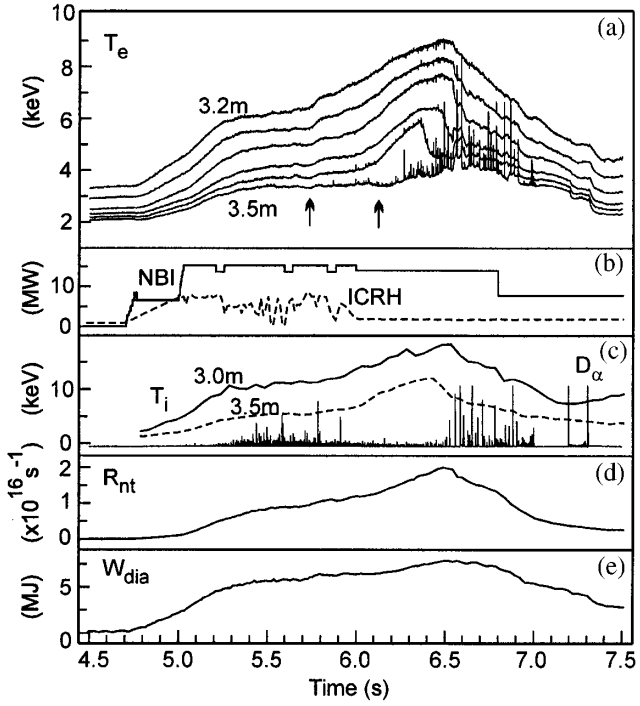

FIG. 1. Time traces of (a) electron temperature at various radial locations, (b) NBI and ICRH power, (c) D_α emission and T_i at core and midradius, (d) neutron rate $R_{\rm nt}$, and (e) stored energy $W_{\rm dia}$ for shot No. 46 727. Arrows mark times of ITB formation.

as well as core) as does the edge magnetic turbulence (from Mirnov coils), scaling in amplitude with heating power.

This is the point in the discharge (5.0 to 5.2 s) where an internal transport barrier would normally form—provided the q profile (which for No. 46 727 drops from above 5 at the edge to just below 2 in the core) has evolved correctly and sufficient heating power is applied [5]. However, because of the uneven ICRH power the ITB does not form until 6.2 s, and then lasts only until 6.5 s when it is terminated by a plasma instability ($q = 2$ snake). At precisely these two times the spectrogram shows an extremely fast collapse and recovery in the high frequency turbulence. There is also a similar drop in high frequency turbulence at 5.7 s coinciding with a sudden rise in the core T_e and T_i (and hence pressure gradient ∇P) and increases in the neutron rate $R_{\rm nt}$ and plasma stored energy $W_{\rm dia}$; see Fig. 1. This might have been the early stages of an ITB but it was not sustained; T_e rises at the edge around 5.9 s and ∇P is reduced.

Although shot No. 46 727 is slightly atypical with its delayed ITB, it clearly illustrates the two distinct stages in the reduction of turbulence. However, the turbulence suppression is by no means global. Lower B_T discharges with strong I_p ramping, such as the $B_T \approx 2.5$ T, $I_p \approx 2.5$ MA discharge No. 46 437 in Fig. 3, where the 75 GHz reflectometer cutoff layer is swept through the ITB region ($R \approx 3.65$ m) to the outboard edge reveal the following: (1) The initial low frequency suppression occurs right across the core out to the ITB foot. (2) The high frequency suppression is restricted to around the narrow ITB gradient region. (3) There is no drop in either the edge density or magnetic turbulence. Note that these individual features are observed in *all* JET optimized shear discharges.

The ITB gradient region is illustrated with the electron temperature T_e (from electron cyclotron emission) and ion temperature T_i [from charge exchange spectroscopy (CXS)] profiles in Fig. 4 during the ITB phase of shot No. 46 727. Both T_e and T_i show steep gradients with foot points which coincide and track each other as the ITB expands and contracts. The difference being that T_i peaks at the magnetic axis while the T_e profile flattens towards the core. The gradient foot also tracks a boundary in the toroidal rotation. Figure 5 is a contour plot of toroidal rotation frequency $\omega_{\rm rot}$ (from CXS) against major radius and time for shot No. 46 727. When the main heating is applied, the plasma core begins to spin up

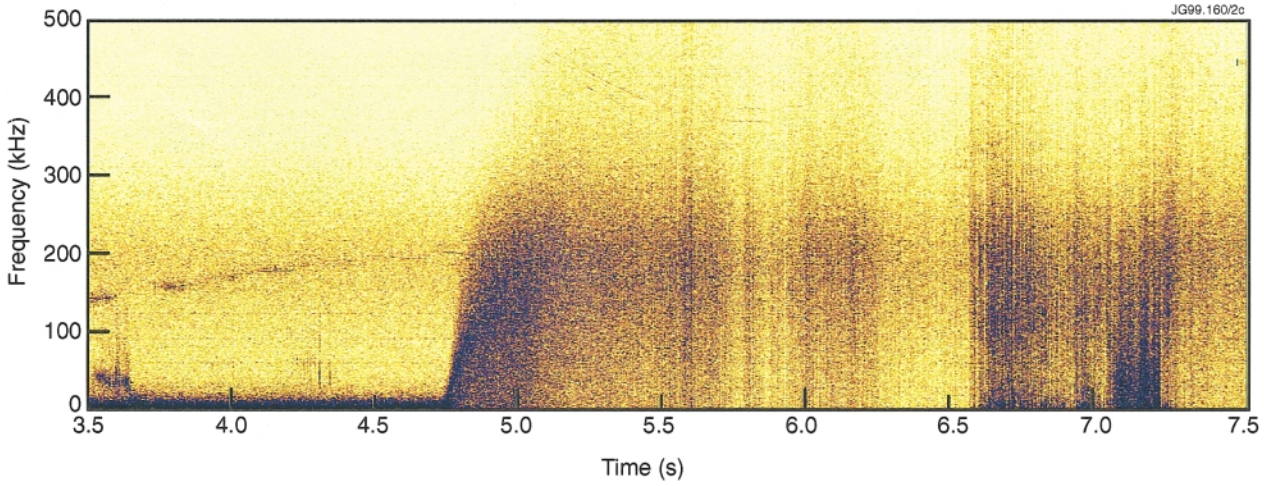

FIG. 2 (color). Spectrogram (log intensity) of density fluctuations ($A\cos\phi$) from a 92 GHz reflectometer channel ($R \approx 3.2$–3.6 m) for shot No. 46 727. N.B. slight background feature around 200 kHz due to amplifier gain anomaly.

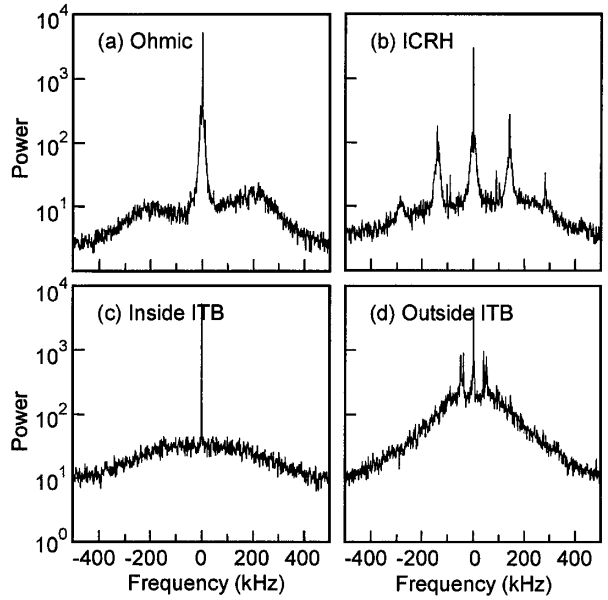

FIG. 3. Spectra from 75 GHz reflectometer channel [$A\exp(i\phi)$ signal] as cutoff layer moves outwards during 2.5 T shot No. 46 437; (a) Ohmic: $R \approx 3.2$ m; (b) ICRH: $R \approx 3.2$ m; (c) inside ITB: $R \approx 3.5$ m; and (d) outside ITB: $R \approx 3.8$ m. The spike at zero frequency is the carrier wave and indicates the level of reflected power.

toroidally (driven by pressure gradient and/or momentum injection), then levels off until the formation of the ITB after 6.0 s. The edge plasma remains virtually stationary throughout the heating phase (confirmed by reflectometer measurements of turbulence propagation velocities of $v < 10\ \mathrm{km\,s^{-1}}$). This generates a region of low velocity shear in the edge, and one of high velocity shear across the core (i.e., semiglobal). The foot of the temperature gradient (marked by crosses) follows the shear boundary (indicated by the change in spacing of the contours).

Since the high shearing region is semiglobal (half minor radius or more) it may be expected to primarily affect fluctuations of similar scale lengths, i.e., very long wavelength. In the Ohmic and L-mode phases reflectometer dispersion relation measurements show the turbulence is dominated by poloidal/toroidal wavelengths from 1 to several meters, i.e., $k_\perp \rho_i \ll 1$. Mode analysis of magnetic signals also confirm this, showing only low toroidal n (e.g., 0, 1, and 2) coherent fluctuations, while the NBI/ICRH phase contains only high $n > 10$ fluctuations, i.e., $k_\perp \rho_i \sim 1$. One explanation is that the velocity shear breaks up the long wavelength turbulence into shorter wavelengths, or that it prevents the normal dissipation/cascade of energy between short and long wavelengths.

This hypothesis that toroidal velocity shear suppresses long wavelengths is also supported by observations of turbulence behavior during other types of discharges. Edge turbulence is reduced during hot ion H-modes when a strong toroidal velocity shear forms at the H-mode pedestal. But during ELMy H-mode discharges this velocity shear is destroyed by the ELMs (edge localized

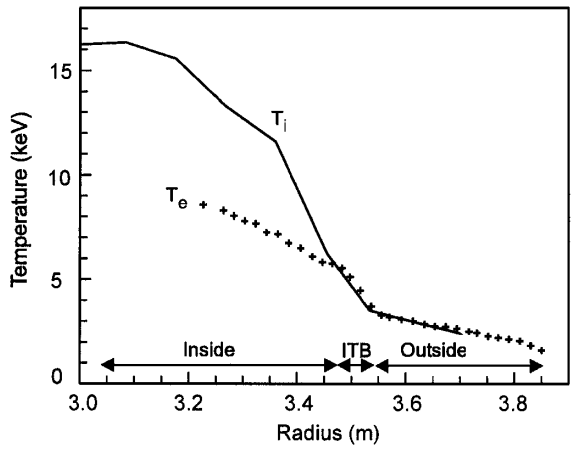

FIG. 4. Radial electron and ion temperature profiles (from a 48 channel heterodyne ECE radiometer and CXS) at 6.28 s during shot No. 46 727. Thermal conductivities $\chi_{i/e}$ are inversely proportional to temperature gradients.

modes) and low frequency edge turbulence is actually enhanced. This is the same situation in the stationary edge region of ITB discharges where the edge turbulence remains high throughout the discharge. If the discharge maintains an L-mode-like edge then the turbulence spectrum is narrow with an exponential shape, while for an ELMy H-mode edge pedestal the spectrum is broader with a bell shape and strong MHD; see Fig. 3(d).

Figures 1 and 2 show that the level of turbulence is related to the fusion performance. The turbulence also appears to be linked with local values of plasma transport. The periods of reduced high frequency turbulence coincide with periods of localized increased electron and ion pressure gradients ∇P_e and ∇P_i at the ITB. This suggests a positive feedback loop [8] in which an increase in the pressure gradient leads to an increase in the poloidal $\mathbf{E} \times \mathbf{B}$ shear, which locally suppresses turbulence (with

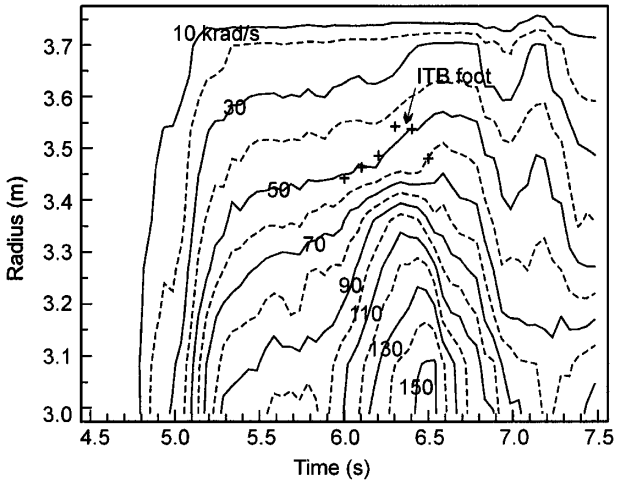

FIG. 5. Contour plot of toroidal angular rotation frequency ω_{rot} from charge exchange spectroscopy v radius and time for shot No. 46 727. Crosses mark position of ITB "foot" from the T_e profile. Contour spacing gives degree of velocity shear.

scale lengths comparable to the ∇P width, i.e., cm wavelengths) which in turn leads to improved confinement and fusion performance, and hence a further increase in ∇P. Positive feedback loops generate fast transitions in state, such as in the measured levels of turbulence. It must be stressed that discharges without ITBs show no high frequency reduction. Further, the level of the high frequency turbulence is correlated with the T_e gradient. The flattening of the T_e profile in the core, Fig. 4, results in electron thermal conductivity χ_e (from TRANSP analysis) dipping at barrier and then rising again in the core [6]—i.e., there is a link between the local χ_e value ($1/\nabla T_e$ at the ITB) and the level of high frequency fluctuations. A similar link has also been observed in TFTR plasmas with enhanced reversed shear [12]. Conversely the suppression of long wavelength fluctuations is correlated with the ion thermal conductivity χ_i ($1/\nabla T_i$). The peaked T_i profile translates to the toroidal rotation increasing towards the core, and χ_i dropping towards neoclassical values at the barrier and then staying low throughout the core. Details of the χ profiles can be seen in Refs. [5,6] for similar ITB discharges.

Improvements in plasma confinement are also accompanied by reductions in turbulent correlation lengths. Reflectometer measurements in the core show a dramatic collapse in the low frequency toroidal coherence, Fig. 6, between the L-mode and main heating phases. Because of the inclination of the magnetic field lines this actually indicates a reduction in the perpendicular (i.e., poloidal) correlation length. Measurements of radial correlation lengths are more difficult due to low levels of signal correlation. Nevertheless, they indicate radial correlation lengths in the core of only a few mm's. These measurements, however, are not inconsistent with the picture of large scale perturbations with poloidally spiraling structures obtained by several authors (e.g., Ref. [13]) using numerical simulations. These structures, while maintaining long spiraling connection lengths, can have narrow radial widths and hence appear to have short instantaneous radial correlation lengths. Velocity shearing could break up these spirals into smaller segments and hence reduce cross-field transport.

To summarize, our results show the following: (1) The formation of a core region of high radial shear in the plasma toroidal velocity (induced by high power NBI and ICRH) is correlated with the suppression of long wavelength turbulence ($k_\perp \rho_i \ll 1$) and with a decrease in the ion thermal conductivity χ_i. (2) The subsequent formation of an internal transport barrier is correlated with a localized suppression of shorter wavelength turbulence ($k_\perp \rho_i \sim 1$) and a coincident localized drop in the electron thermal conductivity χ_e. The behavior of the turbulence suppression

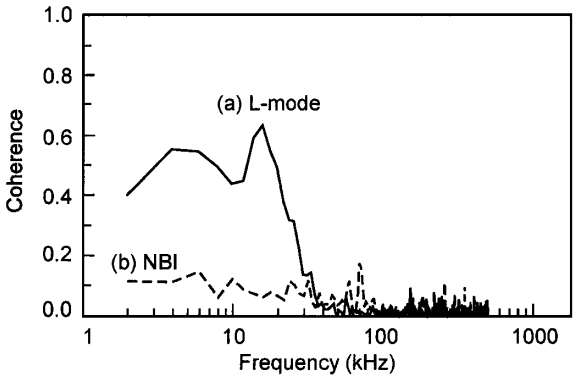

FIG. 6. Coherence spectra between two toroidally separated reflectometer channels (40 mm) during (a) L-mode: $R \approx 3.2$ m; and (b) NBI/ICRH: $R \approx 3.5$ m phases of shot No. 46 423.

is consistent with the theory of a $\mathbf{E} \times \mathbf{B}$ shear positive feedback loop. For the long wavelength suppression the toroidal velocity appears to be the dominant term, while for the shorter wavelengths the ∇P_i term may be more significant. The results present a coherent picture showing the link between long and short wavelength density fluctuations and the ion and electron transport channels, and hence the importance of electrostatic turbulence in the formation of internal transport barriers.

We acknowledge A. Fasoli, R. C. Felton, D. Testa, and R. F. Heeter for assistance with data acquisition, A. Thyagaraja for useful discussions, and members of Task Force B during 1998–1999 and the JET team for the operation of the tokamak.

[1] E. J. Synakowski, Plasma Phys. Controlled Fusion **40**, 581 (1998).
[2] L. L. Lao *et al.*, Phys. Plasmas **3**, 1951 (1996).
[3] C. L. Rettig *et al.*, Plasma Phys. Controlled Fusion **40**, 811 (1998).
[4] E. Mazzucato *et al.*, Phys. Rev. Lett. **77**, 3145 (1996).
[5] C. Gormezano *et al.*, Phys. Rev. Lett. **80**, 5544 (1998).
[6] X. Litaudon *et al.*, Plasma Phys. Controlled Fusion **41**, A733 (1999).
[7] T. Fujita *et al.*, Phys. Rev. Lett. **78**, 2377 (1997).
[8] K. H. Burrell, Phys. Plasmas **4**, 1499 (1997).
[9] G. D. Conway, G. Vayakis, J. A. Fessey, and D. V. Bartlett, Rev. Sci. Instrum. **70**, 3921 (1999).
[10] E. Mazzuccato, Rev. Sci. Instrum. **69**, 2201 (1998).
[11] G. D. Conway, Plasma Phys. Controlled Fusion **41**, 65 (1999).
[12] K. L. Wong *et al.*, Phys. Lett. A **236**, 339 (1997).
[13] Y. Kishimoto *et al.*, Plasma Phys. Controlled Fusion **41**, A663 (1999).